# Anomalous Structure−Activity Relationships of 13-*homo*-13-Oxarotenoids and 13-*homo*-13-Oxadehydrorotenoids

Nianbai Fang, J. Craig Rowlands, and John E. Casida*

*Environmental Chemistry and Toxicology Laboratory, Department of Environmental Science, Policy, and Management, University of California, Berkeley, California 94720-3112*

*Received March 20, 1997*[⊗]

Cubé resin, used as an insecticide/miticide and piscicide, contains in decreasing amounts rotenone (**1**), deguelin (**2**), the 6a,12a-dehydro derivatives of rotenone (**3**) and deguelin (**4**), and the newly-discovered 13-*homo*-13-oxa-6a,12a-dehydro analogs [referred to as oxadehydrorotenone (**5**) and -deguelin (**6**)]. These six rotenoids were compared for potency as inhibitors of NADH:ubiquinone oxidoreductase activity and for organismal toxicity to mosquito larvae, goldfish, and mice and cytotoxicity in three mammalian cell lines (Hepa 1C1C7, MCF 7, and NB 41A3). Although rotenoids **3**−**6** contribute very little to the overall activity of cubé resin, there were two surprising aspects to the structure−activity relationships. First, **1** was 7−15-fold more active than **2** in the cytotoxicity assays of 4-day duration but not in the other systems. This difference in cytotoxicity is not due to specificity at the oxidoreductase target but instead to more extensive cytochrome P450-dependent (piperonyl butoxide-sensitive) detoxification of **2** than of **1**. Second, the observed potency increase on conversion of dehydrorotenone to either rotenone or oxadehydrorotenone suggests that combining both structural changes to form *cis*-13-*homo*-13-oxarotenone (**8**) might result in maximal activity. Accordingly, **5** was reduced with diisobutylaluminum hydride to the *trans*-isomer **7** and then epimerized with aqueous pyridine to the *cis*-isomer **8** of the same configuration as **1**. Surprisingly, **8** was much less active than **1**. This is rationalized on the basis of conformational changes in the B/C ring system and decreasing dihedral angle (determined by X-ray crystallography and/or molecular modeling) between the A and D rings that follow the potency order, *i.e.*, rotenoids **1** and **2** > oxadehydrorotenoids **5** and **6** > *trans*- and *cis*-oxarotenoids **7** and **8** > dehydrorotenoids **3** and **4**. Thus, the novel oxarotenoids and oxadehydrorotenoids help define the conformation optimal for NADH:ubiquinone oxidoreductase inhibition and toxicity.

## Introduction

Cubé resin, an extract of the roots of *Lonchocarpus utilis* and *urucu*, has been used for many decades as an insecticide and piscicide (*1*, *2*). We recently reported that this resin contains not only the major components rotenone (**1**), its α-pyran analog deguelin (**2**), and smaller amounts of their 6a,12a-dehydro derivatives (**3** and **4**, respectively) but also two novel minor ingredients identified as 13-*homo*-13-oxa-6a,12a-dehydrorotenone (**5**) and the corresponding oxadehydrodeguelin (**6**) (*3*) (Figure 1). Compound **5** is bioactive with 50% inhibition of NADH:ubiquinone oxidoreductase activity at 0.11 $\mu$M and of the viability of cells in culture at 4−8 $\mu$M and gives 50% mortality of goldfish at 1 ppm (*3*). Three observations were of particular interest on bioassay of other cubé resin components considered here: first, **1** and **2** are equipotent (except in the cytotoxicity assays); second, rotenoids **1** and **2** are much more active than dehydrorotenoids **3** and **4**; finally, oxadehydrorotenoids **5** and **6** are also generally more active than **3** and **4**. These findings suggesting that *cis*-13-*homo*-13-oxarotenone (**8**) (with the *cis*-B/C ring juncture as in **1**) might be the most active compound of this type. Accordingly, **5** was reduced with diisobutylaluminum hydride (DIBAL-

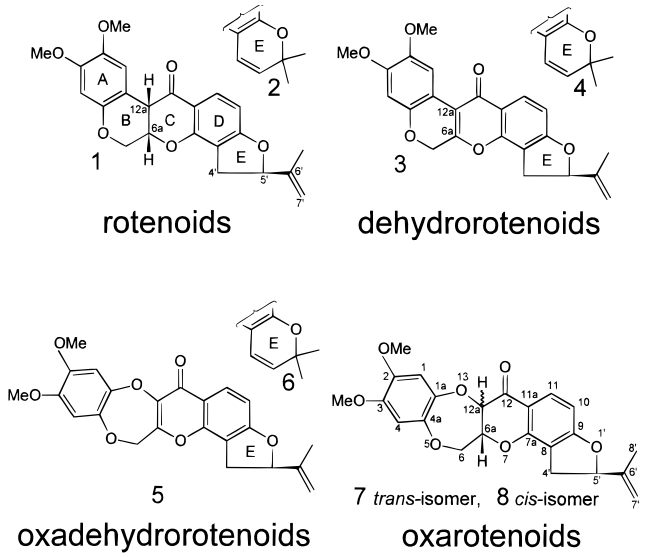


**Figure 1.** Structures of rotenoids **1**−**8** involving four variations of the B/C ring and two of the E ring. Derivatives of **1** referred to in the Discussion but not specifically illustrated are isorotenone with the double bond at 4′,5′ instead of 6′,7′, 12a-methylrotenone with methyl replacing hydrogen at 12a (or the corresponding *trans*-isomer), and 6a,12a-cyclopropylrotenone with a bridge methylene replacing the protons at 6a and 12a.

* To whom correspondence should be addressed. Telephone: (510) 642-5424. Fax: (510) 642-6497. E-mail: ectl@nature.berkeley.edu.

[⊗] Abstract published in *Advance ACS Abstracts,* July 1, 1997.

S0893-228x(97)00043-X CCC: $14.00 

**Table 1. $^1$H NMR (300 MHz) Data ($\delta$) in $CDCl_3$ for 7 and 8[a]**

| proton | 7 | 8 |
|---|---|---|
| 1 (1H) | 6.80 s | 6.69 s |
| 4 (1H) | 6.57 s | 6.60 s |
| 6*eq* (1H) | 4.55 dd ($J$ = 4.1, 13.3) | 4.66 dd ($J$ = 4.4, 13.3) |
| 6*ax* (1H) | 4.45 dd ($J$ = 2.6, 13.3) | 4.19 dd ($J$ = 3.1, 13.3) |
| 6a (1H) | 4.73 ddd ($J$ = 2.6, 4.1, 12.3) | 4.73 m |
| 10 (1H) | 6.58 d ($J$ = 8.7) | 6.59 ($J$ = 8.7) |
| 11 (1H) | 7.84 d ($J$ = 8.7) | 7.85 ($J$ = 8.7) |
| 12a (1H) | 5.06 d ($J$ = 12.3) | 4.38 d ($J$ = 2.1) |
| 4′ (2H) | 3.35 dd ($J$ = 9.7, 15.9) | 3.35 dd ($J$ = 9.8, 15.9) |
| | 2.99 dd ($J$ = 8.2, 15.9) | 3.09 dd ($J$ = 7.7, 15.9 |
| 5′ (1H) | 5.32 dd ($J$ = 8.2, 9.7) | 5.34 dd ($J$ = 7.7, 9.8) |
| 7′ (2H) | 5.10 s | 5.08 s |
| | 4.96 s | 4.94 s |
| 8′ (3H) | 1.78 s | 1.77 s |
| 2-OMe (3H) | 3.83 s | 3.82 s |
| 3-OMe (3H) | 3.82 s | 3.80 s |

[a] $J$ values are given in hertz (Hz).

H)[1] to the *trans*-isomer **7** (*4*) which was epimerized with aqueous pyridine to the *cis*-isomer **8**.

This report compares the contributions of **1**−**6** to the toxicology of cubé resin and the activities of isomers **7** and **8** (Figure 1). Findings from these eight compounds, with some surprising aspects, led to a better understanding of the basis for the difference in cytotoxicity between **1** and **2**, the effects of the B/C ring system on activities of different types, and particularly the importance for activity of the conformation and dihedral angle between the A and D rings.

## Materials and Methods

**Caution**: *Rotenoids include compounds of high toxicity and should therefore be used under containment conditions.*

**Synthesis of *trans*-13-*homo*-13-Oxarotenone (7).** Rotenoids **1**-**6** were isolated from cubè resin (*3*). The procedure used to prepare **7** from **5** was similar to a reported method to convert **3** to the *trans*-isomer of **1** (*4*). Compound **5** used to prepare **7** was obtained by reaction of **1** and acetyl chloride in DMF saturated with oxygen (*3*). To synthesize **7**, a solution of **5** (1.00 g, 2.54 mmol) in dry THF (50 mL) under nitrogen was treated with DIBAL-H in toluene (1.0 M, 6.38 mL) for 1 h at −78 °C. Methanol (30 mL) was added, and the mixture was stirred for 1 h at room temperature. The product was isolated by addition to 1 M hydrochloric acid (50 mL) and extraction with dichloromethane twice (50 mL × 2) followed by preparative TLC on silica gel with toluene:acetone (9:1) to give **7** (530 mg, 53%). Compound **7**: mp 222−224 °C for needles from chloroform and methanol; EI-MS (rel int) 410 $[M]^+$ (100), 227 (6), 219 (2), 213 (9), 203 (8), 193 (7); FAB/MS (rel int) 411 $[M + 1]^+$ (100), 410 (92), 395 (39), 246 (19), 243 (10), 219 (2), 213 (11), 185 (36); HRMS (EI) $m/z$ $C_{23}H_{22}O_7$ 410.1366, found 410.1368; $^1$H and $^{13}$C NMR data are given in Tables 1 and 2.

**Synthesis of *cis*-13-*homo*-13-Oxarotenone (8)**. Compound **8** was prepared by epimerization of **7** (50 mg) on dissolving in pyridine and water (4:1, 10 mL) and heating at 100 °C for 3 h. The solvent mixture was evaporated under nitrogen at 100 °C, and **8** (12 mg, 24%) was isolated by HPLC on a semipreparative column (Econosil silica gel 10 $\mu$m, 10 mm × 25 cm, Alltech, Deerfield, IL) developed with a linear gradient from 21% to 37% ethyl acetate in hexane at a flow rate of 4 mL/min over a period of 40 min monitoring the eluant by UV at 310 nm. Compound **8**: mp 216−218 °C for needles from hexane and ethyl acetate; EI-MS (rel int) 410 $[M]^+$ (100), 227 (4), 219 (8), 213 (14), 203 (16), 193 (17); HRMS (EI) $m/z$ $C_{23}H_{22}O_7$ 410.1366, found 410.1354; $^1$H and $^{13}$C NMR data are given in Tables 1 and 2.

[1] Abbreviations: DIBAL-H, diisobutylaluminum hydride; ETP, electron transfer particles; FAB/MS, fast atom bombardment/mass spectrometry; HRMS, high-resolution mass spectrometry; $IC_{50}$, concentration for 50% inhibition; MTT, 3-(4,5-dimethylthiazol-2-yl)-2,5-diphenyltetrazolium bromide; PB, piperonyl butoxide.

**Table 2. $^{13}$C NMR (75 MHz) Data ($\delta$) in $CDCl_3$ for 7 and 8**

| carbon | 7 | 8 |
|---|---|---|
| 1 | 114.1 | 113.5 |
| 1a | 142.4 | 143.8 |
| 2 | 144.8 | 145.3 |
| 3 | 145.1 | 145.3 |
| 4 | 104.8 | 105.2 |
| 4a | 141.7 | 143.1 |
| 6 | 73.3 | 71.8 |
| 6a | 79.7 | 78.6 |
| 7a | 157.5 | 158.0 |
| 8 | 113.2 | 113.1 |
| 9 | 167.1 | 167.7 |
| 10 | 105.2 | 105.5 |
| 11 | 129.8 | 130.3 |
| 11a | 104.9 | 105.5 |
| 12 | 187.4 | 184.4 |
| 12a | 79.8 | 78.9 |
| 4′ | 31.2 | 31.1 |
| 5′ | 87.8 | 88.1 |
| 6′ | 142.9 | 143.0 |
| 7′ | 112.7 | 112.7 |
| 8′ | 17.0 | 17.0 |
| 2-OMe | 56.3 | 56.2 |
| 3-OMe | 56.3 | 56.2 |

**Inhibition of NADH:Ubiquinone Oxidoreductase Activity.** NADH:ubiquinone oxidoreductase activity of bovine heart electron transport particles (ETP) (*5*) was assayed by the standard procedure (*6*). The ETP (40 $\mu$g of protein) and candidate inhibitor (added in 10 $\mu$L of $Me_2SO$) in 50 mM potassium phosphate buffer at pH 7.4 (1.0 mL) were preincubated for 5 min at 25 °C. The residual enzyme activity was determined by adding NADH and immediately and continuously monitoring the loss of absorbance at 340 nm for 3 min at 25 °C with a Hewlett-Packard 8452A diode array spectrophotometer. The slope of the line was compared for a sample with inhibitor to that for the control without inhibitor to obtain the percentage inhibition. Assays were also made for inhibition of NADH: ubiquinone oxidoreductase activity in the crude mitochondrial fraction (300 $\mu$g of protein) isolated according to the method of Bourgeron *et al.* (*7*) from $1 \times 10^8$ Hepa 1C1C7 cells (see below). The concentration for 50% inhibition ($IC_{50}$) was determined from two or more experiments with duplicate samples using a 1, 3, 10, 30, etc., nM concentration series.

**Organismal Toxicity.** $LD_{50}$ values were determined for the rotenoids from cubè resin using an insect, a fish, and a mammal. Ten first-instar mosquito larvae (*Aedes aegypti* L.) (eggs provided by William Reisen and Thomas Scott of the Arbovirus Field Station, University of California, Bakersfield, CA) were placed in 1 mL of water containing the test compound added in 10 $\mu$L of $Me_2SO$. The mortality end point at 24 h was considered to be an inability of the larvae to move in response to a strong light source (*8*). Goldfish (1.6−2.1 g) were individually placed in 300 mL of deionized water bubbled continuously with air. The test compound was added in ethanol (100 $\mu$L) and mortality determined at 24 h. Mouse toxicity (male Swiss-Webster albino, 17−20 g) was assayed by ip treatment with the test compound in $Me_2SO$ (10−100 $\mu$L) with mortality determined at 24 h (all mortality observed was within the first 2 h). The $LD_{50}$ values from log-probit plots were reproducible within 2-fold in repeated experiments.

**Cytotoxicity**. Three cell lines, mouse liver cancer cells (Hepa 1C1C7) (Tissue Culture Facility, Department of Molecular and Cell Biology, University of California at Berkeley), human epithelial breast cancer cells (MCF 7), and mouse neuroblastoma cells (NB 41A3) (American Type Culture Collection, Rockwell, MD), were maintained in Dulbecco's modified Eagle's medium (pH 7.3) supplemented with 0.37% $NaHCO_3$, 5% fetal bovine serum, and 0.1% penicillin/streptomycin at 37 °C in a humidified atmosphere of 5% $CO_2$/95% air. Cells were added to 96-well microplates with 5000 cells in 100 $\mu$L of medium/well and incubated for 24 h. Test chemicals were dissolved in $Me_2SO$ ($Me_2SO$ alone as control), mixed with 100 $\mu$L of medium, and then added to each well (200 $\mu$L/well total volume, 0.4% final $M_2SO$ concentration), and cell viability was

**Table 3. Biological Activities of Rotenoids, Oxadehydrorotenoids, and Dehydrorotenoids**

| | rotenoid | | oxadehydrorotenoid | | dehydrorotenoid | |
|---|---|---|---|---|---|---|
| assay | rot[a] (**1**) | deg[a] (**2**) | rot (**5**) | deg (**6**) | rot (**3**) | deg (**4**) |
| NADH:ubiquinone oxidoreductase, $IC_{50}$ (nM) | | | | | | |
| beef heart ETP | 4.4 ± 1.4 | 6.9 ± 0.9 | 115 ± 16 | 138 ± 38 | 8625± 25 | 1590 ± 210 |
| organismal toxicity, $LD_{50}$ | | | | | | |
| mosquito larvae (ppm)[b] | 2.6 ± 0.6 | 3.2 ± 0.3 | >100 (12 ± 4) | >100 (2 ± 2) | >100 (5 ± 3) | 64 ± 29 |
| goldfish (ppm) | 0.05 | 0.03 | 1.0 | >3.0 | >3.0 | >3.0 |
| mouse, ip (mg/kg) | 2.5 | 5.0 | >50 | >50 | >50 | >50 |
| cytotoxicity, $IC_{50}$ ($\mu$M)[c] | | | | | | |
| Hepa 1C1C7 | 0.24 ± 0.04 | 3.4 ± 0.3 | 7.6 ± 0.2 | 5.3 ± 1.8 | >30, >30 | 7.5, >30 |
| MCF 7 | 0.35 ± 0.06 | 5.3 ± 1.4 | 4.1 ± 0.8 | 15 ± 0.7 | 27, >30 | 10, >30 |
| NB 41A3 | 0.38 ± 0.02 | 2.5 ± 0.6 | 4.2 ± 0.6 | 8.4 ± 2.0 | 12, >30 | 7.2, >30 |

[a] Rotenone and deguelin series are abbreviated rot and deg. [b] $LD_{50}$ as mean ± SE ($n$ = 3) or percentage mortality at 100 ppm (in parentheses). The potency of **1** and **2** was altered less than 2-fold by PB at 1 or 2 ppm. Compounds **3**−**6** at 30−100 ppm precipitated within the first 2 h of the assay. [c] Values are mean ± SE ($n$ = 4 with two MTT and two acid phosphatase assays) or mean of two experiments for MTT assay followed by mean of two experiments for acid phosphatase assay.

determined after 72 h incubation. In a special experiment with Hepa cells and the 3-(4,5-dimethylthiazol-2-yl)-2,5-diphenyltetrazolium bromide (MTT) assay (*9*), rotenone and deguelin were assayed alone and in the presence of the P450 oxidase inhibitor piperonyl butoxide (PB) at 0.5, 2.5, or 12.5 $\mu$M (which was not toxic in itself).

One cytotoxicity assay involved addition to each well of MTT (125 $\mu$g) (Sigma) in 50 $\mu$L medium as above containing 5% $Me_2SO$. After 4 h incubation, the medium was carefully removed by aspiration, the formazan precipitate dissolved in 100 $\mu$L of $Me_2SO$, and the absorbance determined at 570 nm. A second cytotoxicity determination evaluated activity as absorbance at 410 nm for *p*-nitrophenate ion liberated on hydrolysis of *p*-nitrophenyl phosphate (Sigma) (*10*). Absorbances were measured with the $UV_{max}$ kinetic microplate reader (Molecular Devices, Menlo Park, CA). Each cytotoxicity assay in duplicate involved at least five concentrations of the test compound in a 1, 3, 10, 30, etc., $\mu$M series with the $IC_{50}$ value determined by log-probit plot of concentration versus absorbance of the formazan or nitrophenate ion.

**X-ray Crystallography**. Crystal data for **6**: $C_{23}H_{20}O_7$, $M$ = 408.39; monoclinic; $a$ = 28.107(3), $b$ = 7.3007(7), and $c$ = 19.0778(12) Å; $\beta$ = 105.278 (6)°, $V$ = 3776.4(6) Å$^3$, Z = 8, $D_c$ = 1.437 mg m$^{-3}$; $F(000)$ = 1712; space group $C2/c$, crystal size 0.40 × 0.16 × 0.01 mm. The selected crystal of **6** was mounted in the cold stream (130 K) of a Siemens P4 diffractometer equipped with a LT-2 low-temperature apparatus. The radiation employed was Ni-filtered Cu Kα from a Siemens rotating anode source operating at 15 kW. The structure was solved using direct methods (SHELXTL, version 5.03) in the centrosymmetric space group $C2/c$. Hydrogens were added geometrically and refined using a riding model. An empirical absorption correction [XABS2 (*11*)] was applied. Final refinement was by full-matrix least-squares methods, based on $F^2$, using all data and with anisotropic thermal parameters for non-hydrogen atoms. The largest peaks in the final difference map were less than 0.32 e Å$^{-3}$. Final $R$ indices are w$R2$ = 0.0628 (all 2469 data) and $R1$ = 0.0486 [calculated based on 1960 observed (>2$\delta(I)$) data].

On a similar basis, the structure of **1** was solved using direct methods in the space group $P2_12_12_1$. There were two molecules in the asymmetric unit identical to those reported earlier (*12*), and one of these displayed minor disorder in the vinyl group apparently due to a different conformation of the dihydrofuranyl ring. The atomic coordinates and equivalent isotropic displacement parameters, bond lengths and angles, anisotropic displacement parameters, and hydrogen coordinates and isotropic displacement parameters for **1** and **6** are available from the Cambridge Crystallographic Data Centre (12 Union Rd, Cambridge, CB2 1EZ, U.K.), and other information is available from the University of California at Davis.

**Molecular Modeling.** Compounds **1**, **5**, **7**, and **8** were modeled by a stochastic search method based on a molecular mechanics program using the standard MM2 procedure (*13, 14*)[2] yielding several conformations for each molecule. The lowest energy conformations were used for **1** and **7**, and the second lowest energy one was used for **8** (ignoring the puckering in the dihydrofuranyl ring), but this molecular mechanics procedure yielded only flat conformers for **5,** inconsistent with accurate Dreiding models for this compound, possibly arising from electronic affects that the MM2 procedure does not take into account. Accordingly, the molecular orbital package MOPAC, using the semiempirical AM1 Hamiltonian, was applied to **5** yielding a local minimum which was only 0.76 kcal/mol above the global minimum (in AM1 terms).

## Results

**Structural Assignments for Synthetic 7 and 8.** The structures were assigned by $^1$H and $^{13}$C NMR (Tables 1 and 2). The hydrogens at C-6a and C-12a in **7** and **8** were also confirmed by comparing their $^1$H NMR spectra (Table 1) with that of **5** (*3*). Since the coupling constant for the 6a and 12a protons is 12.8 Hz for *trans*-rotenone and 3.9 Hz for *cis*-rotenone (**1**) (*4*), the corresponding 12.3 Hz coupling of **7** confirmed the *trans*-B/C fusion and the 2.1 Hz coupling of **8** indicated the *cis*-isomer of **7** (Table 1). Assignment of the configuration as (6a*S*,12a*S*,5′*R*)-**7** follows from its similar optical rotation (−94.0, $CHCl_3$, $c$ = 1) to that of (6a*S*,12a*S*,5′*R*)-**1** (−111.5, $CHCl_3$, $c$ = 1) as the standard. Epimerization at C-12a was supported by the large shift of the H-12a resonance from downfield ($\delta$ 5.06 ppm) for **7** to upfield ($\delta$ 4.38 ppm) on conversion to **8** (*4*). The major product in the reduction of **5** is therefore (6a*S*,12a*R*,5′*R*)-**7**.

**Effect of Rotenoid Structure on Bovine NADH: Ubiquinone Oxidoreductase Inhibition and Organismal Toxicity**. The high potency of **1** as an oxidoreductase inhibitor is shared by **2**, and in each case their potency is reduced 20−26-fold as the oxadehydro analogs **5** and **6** and 230−1960-fold as the dehydro derivatives **3** and **4** (Table 3). The similar potency of the rotenone and deguelin series and the same order of rotenoid > oxadehydrorotenoid > dehydrorotenoid extend to their organismal toxicity, *i.e.*, mosquito larvae, goldfish, and mice (Table 3). Although the potency is increased on conversion of dehydrorotenone (**3**) to either rotenone (**1**) or oxadehydrorotenone (**5**), the incorporation of both structural changes to form *cis*-oxarotenone (**8**) or its *trans*-isomer **7** gives an anomalous structure−activity relationship, in that they are much less potent than anticipated as oxidoreductase inhibitors and toxicants (Table 4).

[2] The molecular mechanics program (referred to as AESOP and developed by B. B. Masek, Zeneca, Wilmington, DE) was derived in part from BIGSTRN-3 (QCPE 514) (*13*) employing the MM2 force field parameters (*14*).

**Table 4. Correlation for Rotenone Derivatives between Bioactivity and Conformation**

| parameter | compounds 1 | 5 | 7 | 8 | 3 |
|---|---|---|---|---|---|
| bioassay, $IC_{50}$ | | | | | |
| NADH:ubiquinone oxidoreductase (nM) | 4.4[a] | 115[a] | 730 | 2600 | 8625[a] |
| Hepa cell line ($\mu$M)[b] | 0.28 | 7.8 | 7.1 | 25 | >30 |
| mouse, ip, $LD_{50}$ (mg/kg) | 2.5 | >50 | >50 | >50 | >50 |
| dihedral angle (deg) | | | | | |
| X-ray | 91 | 133 | | | |
| model | 106 | 136 | 149 | 145[c] | 180[d] |

[a] Data from Table 3. [b] Mean of two experiments for MTT assay. Data in Table 3 are means of MTT and acid phosphatase assays. [c] Twist conformation shown in Figure 4. [d] A and D rings in conjugation with C-12 carbonyl group.

**Effect of Rotenoid Structure on Cytotoxicity**. The three cell lines are not greatly different in their sensitivity to **1** but are much less sensitive to rotenoids **2**−**6** (Tables 3 and 4). *trans*-Oxarotenone (**7**) is similar in activity to oxadehydrorotenone (**5**), whereas the *cis*-isomer **8** is much less active (Table 4). Thus, within the rotenone series the cytotoxic potency decrease of rotenone > oxadehydrorotenone ≥ oxarotenone > dehydrorotenone parallels that for the oxidoreductase and organisms above. The structure−activity relationships are similar for the rotenone and deguelin series, where data are available, with one marked exception, *i.e.*, deguelin itself is much less active (7−15-fold) than rotenone (Table 3).

**Mechanism for Difference in Cytotoxicity of Rotenone and Deguelin**. The lower potency of **2** than **1** in the cytotoxicity assays (*e.g.*, 14-fold in the Hepa cells) but not in the other systems might be due to (a) lower sensitivity in the cells of the oxidoreductase target or (b) slower penetration or more rapid detoxification of **2** than **1**. The first hypothesis involves a specificity difference for the oxidoreductase from beef heart and the cell lines. Accordingly, the potencies of **1** and **2** were compared with the crude mitochondrial fraction of Hepa 1C1C7 cells. Rotenone has about 2 times the potency of deguelin with $IC_{50}$s for the rotenone-sensitive oxidoreductase activity of 0.6 ± 0.2 and 1.2 ± 0.4 nM and for the total oxidoreductase activity of 2.6 and 5.6 nM, respectively, ruling against the importance of target site specificity. The penetration and detoxification proposal was tested by including PB at 0.5−12.5 $\mu$M in the cytotoxicity assays leading at the highest level to a 10-fold potency increase for **2** and a 2.3-fold increase for **1** (Figure 2), thereby favoring the detoxification hypothesis.

**Conformations of Rotenoids.** The stereochemistry and conformations of **1**, **5**, and **6** were determined by X-ray crystallography. Rotenone (**1**) in crystal form appears as two conformers, of which the V-shaped conformation was predicted to be the more stable at room temperature by molecular mechanics techniques (*12*) and was the only one present in solution (*4*). Furthermore, the B and C ring conformations of **1** and **2** in solution are identical suggesting that **2** is also the V-shaped conformation (*15*). Compound **5** has statistical disorder in the rotational conformation of the vinyl group, but this disorder does not affect the other atoms of the molecule (*3*). The conformations of **5** and **6** are similar to each other (Figure 3). The bent nature of these molecules, conveniently quantified in terms of the dihedral angle between the two aromatic rings (A and D), was therefore evaluated as a factor in relating three-dimensional structure and bioactivity of the rotenoids.

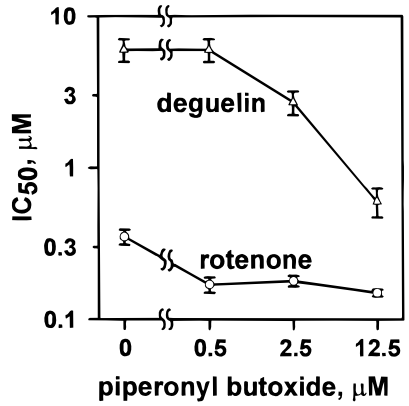


**Figure 2.** Differential effect of the P450 inhibitor PB on the cytotoxicity of rotenone (**1**) and deguelin (**2**). The $IC_{50}$ values for **1** and **2**, respectively, are 0.35 ± 0.04 and 6.0 ± 0.1 $\mu$M without PB and 0.15 ± 0.01 and 0.60 ± 0.13 $\mu$M with 12.5 $\mu$M PB.

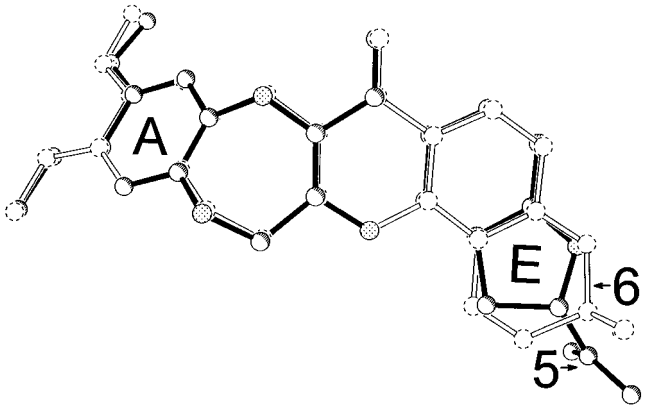


**Figure 3.** Comparison of the conformations of rotenoids **5** and **6** with different E rings based on X-ray crystal structures. This is the first crystal structure reported for a rotenoid with a *gem*-dimethylpyran moiety.

To determine the effect of the B/C ring system on the conformation, compounds **1**, **7**, and **8** were modeled using the standard molecular mechanics procedure and **5** by the quantum mechanics approach (Figure 4). It is noteworthy that the fully-optimized structure for **1** obtained by the MM2 method was not significantly different from the crystal structure determined by X-ray and that the conformation for **5** was consistent with the X-ray structure except for the conformation of the B ring. Also, examination of NMR data for **8**, based on the corresponding data for **1** (*15*), suggests a predominant conformation which is similar to that obtained from the standard MM2 procedure (*13, 14*).[2] These comparisons support the validity of the computer-generated models. The decreasing dihedral angle (determined by X-ray crystallography and molecular modeling) between the A and D rings generally follows the potency order (Table 4).

## Discussion

The E ring and the B/C ring system have a major influence on the bioactivity of constituents in cubè resin which is due predominantly to **1** with some contribution from **2** but little if any from **3**−**6**, which all have the same A and D rings. However, an anomalous structure−activity relationship became apparent for these cubè resin constituents (**1**−**6**) and their oxarotenone analogs (**7** and **8**) in that dehydrogenation at 6a and 12a greatly reduces the potency of the rotenoids but increases that

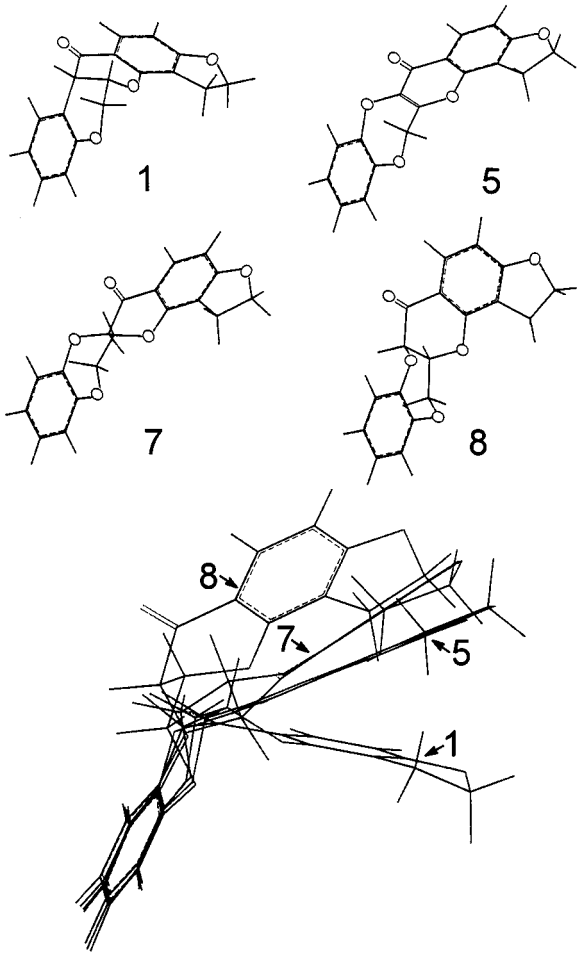


**Figure 4.** Computer-generated models of **1**, **7**, and **8** based on molecular mechanics and of **5** derived from the quantum mechanics approach. The conformations of models for **1** and **5** were consistent with those of their crystal structures (see text). Substituents of the A and E rings are deleted for ease of comparisons. Conformations for **1**, **5**, **7**, and **8** shown individually at the top are superimposed relative to the A ring in the composite figure at the bottom.

of the oxarotenoids. This does not involve a change in the mode of action. Thus, the finding of similar structure−activity relationships for inhibition of NADH:ubiquinone oxidoreductase activity and for toxicity to an insect, a fish, a mammal, and three cell lines suggests that inhibition of oxidoreductase activity is probably associated with toxicity in each case. Possible mechanisms by which the E ring and the B/C ring system influence the potency of these rotenoids are considered below.

The E ring confers almost identical overall molecular conformation in the rotenone and deguelin series based on X-ray crystal structure analysis (this study) and NMR data in solution for **1** and **2** (*15*). The rotenone and deguelin series are similar in potency in all assays with the single marked exception of cytotoxicity in which rotenone is 7−15-fold more potent than deguelin. This is not due to target site specificity since rotenone and deguelin are similar in potency for inhibition of NADH: ubiquinone oxidoreductase activity, not only from bovine heart but also in the crude mitochondrial fraction of Hepa 1C1C7 cells. An alternative hypothesis involves faster detoxification of deguelin than rotenone during the cytotoxicity assay. Rotenone is metabolized by PB-sensitive liver P450s primarily by oxidation at the 12a position and the isopropenyl side chain (*16*), and its toxicity to mice is greatly increased by inactivation of these P450s by PB (*17*). In the present study with Hepa cells, PB synergized both compounds and reduced the potency difference between **1** and **2** from 17-fold without PB to 4-fold with PB. The lower synergism of rotenone than deguelin in the cells is consistent with a less rapid P450-dependent detoxification for the isopropenylfuran than the dimethylpyran substituent, a possibility not examined directly in this investigation. The large potency difference between rotenone and deguelin appears only in the cell assays of 4-day duration and not in the organismal toxicity in much shorter assays where the relative detoxification rates may not be major limiting factors in the potency. It appears therefore that the potency difference of rotenone and deguelin in the cell assays is due to their relative detoxification rates rather than target site specificity.

The bioactivity of the rotenoids examined here may be related to their overall molecular conformation determined by the B/C ring system. It is not related to the presence or absence of a proton at position 6a or 12a because dehydrogenation at 6a or 12a can either decrease or increase potency depending on the B/C ring system. This study establishes that the potency order for analogs in the rotenone series as NADH:ubiquinone oxidoreductase inhibitors and toxicants generally follows their dihedral angles between the A and D rings. The preferred conformation is the bent [referred to as ridge-tile-like (*4*)] structure of rotenone rather than a larger angle. The stereochemistry at the B/C ring junction (*cis* versus *trans*) also greatly influences the biological activity. (±)-*cis*-Isorotenone (Figure 1) has a bent V-shaped structure, whereas the *trans*-conformation is flatter and more extended, *i.e.*, the angles between the A and D rings are 99° and 101° for each of the crystallographically-distinct *cis*-molecules and 158° for the *trans*-molecule (*4*). In 12a-methylrotenone (Figure 1), with a blocked B/C ring system, the *cis*-isomer is more effective than the *trans* as a NADH:ubiquinone oxidoreductase inhibitor and insecticide, and the reported activity of the labile *trans*-rotenone or -isorotenone (*18*) may be due to epimerization to the more stable *cis*-geometry under the assay conditions (*18*, *19*). The conformation of 6a,12a-cyclopropylrotenone (Figure 1) is intermediate between the V-shaped *cis*-12a-methylrotenone and the planar *trans*-isomer, and its potency is, as expected, between that of *cis*- and *trans*-12a-methylrotenone (*19*). 13-*homo*-13-Oxarotenone is the only case in which the *trans*-isomer (which is much more stable than *trans*-rotenone; see ref 4) is more potent that the *cis*-counterpart. Thus, the novel oxarotenoids and oxadehydrorotenoids described here help define the best conformation conferred by the B/C ring system to position the A ring and the D/E ring system for optimal NADH: ubiquinone oxidoreductase inhibition and toxicity.

**Acknowledgment.** We thank our laboratory colleagues Wei-Wei Li, Phillip Jefferies, and Gary Quistad for advice and assistance. Thomas Singer of the University of California at San Francisco provided the electron transport particles. Crystallographic analyses were conducted by Marilyn Olmstead of the Department of Chemistry, University of California at Davis. We are especially indebted to Harold Cox of the Agricultural Products Division, Zeneca Inc. (Richmond, CA), for molecular modeling and conformational analysis. The project described was supported by Grant P01 ES00049 from the National Institute of Environmental Health Sciences, NIH.

## References

(1) Roark, R. C. (1941) Present status of rotenone and rotenoids. *J. Econ. Entomol.* **34**, 684−692.

(2) Negherbohn, W. O. (1959) *Handbook of Toxicology, Volume III: Insecticides*, pp 661−673, W. B. Saunders Co., Philadelphia, PA.

(3) Fang, N., and Casida, J. E. (1997) Novel bioactive cubè insecticide constituents: isolation and preparation of 13-*homo*-13-oxadehydrorotenoids. *J. Org. Chem.* **62**, 350−353.

(4) Begley, M. J., Crombie, L., Hadi, A., Hamid bin, A., and Josephs, J. L. (1993) Synthesis of *trans*-B/C-rotenoids: X-ray and NMR data for *cis*- and *trans*-forms of isorotenone. *J. Chem. Soc., Perkin Trans.* **1**, 2605−2613.

(5) Crane, F. L., Glenn, J. L., and Green, D. E. (1956) Studies on the electron transfer system. IV. The electron transfer particle. *Biochim. Biophys. Acta* **22**, 475−487.

(6) Wood, E., Latli, B., and Casida, J. E. (1996) Fenazaquin acaricide specific binding sites in NADH: ubiquinone oxidoreductase and apparently the ATP synthase stalk. *Pestic. Biochem. Physiol.* **54**, 133−145.

(7) Bourgeron, T., Chretien, D., Rötig, A., Munnich, A., and Rustin, P. (1992) Isolation and characterization of mitochondria from human B lymphoblastoid cell lines. *Biochem. Biophys. Res. Commun.* **186**, 16−23.

(8) Casida, J. E. (1955) Toxicity of aromatic acids to the larvae of the mosquito *Aedes aegypti* L. and the counteracting influence of amino acids. *Biochem. J.* **59**, 216−221.

(9) Cohen, E., Quistad, G. B., and Casida, J. E. (1996) Cytotoxicity of nimbolide, epoxyazadiradione and other limonoids from neem insecticide. *Life Sci.* **58**, 1075−1081.

(10) Connolly, D. T., Knight, M. B., Harakas, N. K., Wittwer, A. J., and Feder, J. (1986) Determination of the number of endothelial cells in culture using an acid phosphatase assay. *Anal. Biochem.* **152**, 136−140.

(11) Parkin, S., Moezzi, B., and Hope, H. (1995) XABS2: an empirical absorption correction program. *J. Appl. Crystallogr.* **28**, 53−56.

(12) Rossi, M., Fule, P. Z., and Taylor, M. R. (1988) Conformational flexibility in the molecular structure of rotenone, a naturally occurring insecticide. *Bioorg. Chem.* **16**, 376−387.

(13) Nachbar, R. B., Jr., and Mislow, K. (1986) BIGSTRN-3: General-purpose empirical force-field program. *QCPE Bull.* **6**, 96−97.

(14) Allinger, N. L., and Yuh, Y. H. (1980) MM2: Molecular mechamics II. *QCPE Bull.* **12**, 395.

(15) Carlson, D. G., Weisleder, D., and Tallent, W. H. (1973) NMR investigations of rotenoids. *Tetrahedron* **29**, 2731−2741.

(16) Fukami, J.-I., Yamamoto, I., and Casida, J. E (1967) Metabolism of rotenone in vitro by tissue homogenates from mammals and insects. *Science* **155**, 713−716.

(17) Škrinjarić-Špoljar, M., Matthews, H. B., Engel, J. L., and Casida, J. E. (1971) Response of hepatic microsomal mixed-function oxidases to various types of insecticide chemical synergists administered to mice. *Biochem. Pharmacol.* **20**, 1607−1618.

(18) Begley, M. J., Crombie, L., Hadi, A., Hamid bin, A., and Josephs, J. L. (1990) Synthesis and comparison of unnatural *trans*-B/C rotenoids with the natural *cis*-stereoisomers. In *Pesticides and Alternatives* (Casida, J. E., Ed.) pp 311−315, Elsevier, New York.

(19) Josephs, J. L., and Casida, J. E. (1992) Novel synthetic rotenoids with blocked B/C ring systems. *Bioorg. Med. Chem. Lett.* **2**, 593−596.

TX9700432